J Mater Sci: Mater Electron (2017) 28:2435–2441
DOI 10.1007/s10854-016-5815-4

Simultaneously enhanced ferroelectric and magnetic properties in $0.675BiFe_{1-x}Cr_xO_3$–$0.325PbTiO_3$ ($x = 0$–0.05) ceramics

Xian-Zhu Deng[1] · Ji Zhang[1] · Shan-Tao Zhang[1]

Received: 15 June 2016 / Accepted: 3 October 2016 / Published online: 11 October 2016

Abstract Multiferroic ceramics of $0.675BiFe_{1-x}Cr_xO_3$–$0.325PbTiO_3$ ($x = 0$, 0.01, 0.025, 0.05) were prepared and comparatively investigated. The rhombohedral–tetragonal morphotropic phase boundary (MPB) was formed in $0.675BiFeO_3$–$0.325PbTiO_3$. The B-site Cr-substitution changes the structure from MPB to rhombohedral phase gradually, accompanied with monotonously decreased ferroelectric Curie temperature and average grain size. More interestingly, Such Cr-substitution enhances room temperature ferroelectric and magnetic properties simultaneously. The underlying mechanism is mainly attributed to the substitution enhanced local Fe^{3+}–Cr^{3+} magnetic interaction and the suppressed oxygen vacancy effect. We believe these results are helpful supplements for optimizing structures and room temperature multiferroic properties of $BiFeO_3$-based materials.

1 Introduction

Multiferroic materials are compounds which exhibit at least two ferroic properties simultaneously [1–3]. Single phase multiferroics have been attracted great interests for the rich physical properties and huge application potential [4, 5]. Bismuth ferrite ($BiFeO_3$) is a promising single phase multiferroicperovskite oxide with rhombohedral structure. The lone pair electrons of A-site Bi^{3+} induced structural distortion, which causes ferroelectricity (Curie temperature, $T_c \sim 830$ °C), while B-site Fe^{3+} provides the antiferromagnetic order (Néel temperature, $T_N \sim 370$ °C) [6–9]. For a long time, the weak magnetic property and high conductivity have been the obstacle preventing the intrinsic investigation and the possible applications of $BiFeO_3$. In order to solve these problems, many attempts such as A-site or B-site substituting have been carried out [10–18]. Such A- or B-site substituting can enhance magnetic [19–22]. Furthermore, A- and B-site co-substituting, i.e., forming solid solution with other ABO_3 type of perovskites, is also an effective way to enhance the resistivity and improve magnetization [23]. It is noted that the above methods can enhance magnetic property but generally result in decreased ferroelectric T_c and/or suppressed ferroelectricity [24, 25], which means it is relatively difficult to enhance ferroelectric and magnetic properties simultaneously.

Accordingly, to further optimize and enhance room temperature ferroelectric and magnetic properties of $BiFeO_3$-based materials simultaneously, a possible way is to carry out appropriate substituting starting from an appropriate $BiFeO_3$-based solution which has good ferroelectric property with high ferroelectric T_c. Fortunately, $BiFeO_3$-base solid solution of $(1-x)BiFeO_3$–$xPbTiO_3$ is reported to have large remnant polarization ($P_r \sim 62$ μC/cm^2) and high ferroelectric T_c (~ 700 °C, $x = 0.2$) after quenched [26, 27]. Actually, $(1-x)BiFeO_3$–$xPbTiO_3$ solid solutions, especially the compositions near rhombohedral–tetragonal morphotropic phase boundary ($x = 0.3$–0.35), have been widely investigated in the past few years mainly due to the high ferroelectric/piezoelectric performances. However, the $(1-x)BiFeO_3$–$xPbTiO_3$ still shows antiferromagnetic nature [28]. This means magnetic property of $(1-x)BiFeO_3$–$xPbTiO_3$ needs further optimizing, in order

✉ Shan-Tao Zhang
stzhang@nju.edu.cn

[1] National Laboratory of Solid State Microstructures and Department of Materials Science and Engineering, College of Engineering and Applied Science, Nanjing University, Nanjing 210093, China

to develop multiferroic materials with excellent room temperature ferroelectric and magnetic properties.

Up to now, some chemical doped/substituted $BiFeO_3$–$PbTiO_3$ have been reported [28, 29]. As described above, enhanced magnetic property is generally at the expense of suppressed ferroelectric property. Therefore, it is still a challenge to enhance ferroelectric and magnetic properties simultaneously in single phase solid solution. Though forming ferroelectrics-magnetic oxide composite structure, i.e., magnetic oxide is embedded into the ferroelectric matrix, can achieve this goal [30], the magnetoelectric interaction in such composite is not intrinsic and thus is not interesting from viewpoint of fundamental science. So, searching for new chemical substituted $(1-x)BiFeO_3$–$xPbTiO_3$with simultaneously enhanced ferroelectric and magnetic properties is still of great interest.

Actually, enhancing multiferroic property is greatly dependent on the ions used for chemical substituting because some cations favor to form ferromagnetic interaction. We note that neighboring Fe^{3+}–Cr^{3+} (Fe^{3+}: $3d^5$, $S = 5/2$, Cr^{3+}: $3d^3$, $S = 3/2$) cations favor ferromagnetic interaction with a large net magnetization, as evidenced by the magnetization of 8.0 μ_B per Fe^{3+}–Cr^{3+} pair and a high ferromagnetic Curie temperature of 375 K observed in the artificial superlattice constructed by G-type antiferromagnetic $LaFeO_3$ and $LaCrO_3$ [31, 32]. Theoretical calculation also shows that even neighboring Fe^{3+}–Cr^{3+} pair posses antiferromagnetic interaction, the net magnetization is still as high as 2.0 μ_B per Fe^{3+}–Cr^{3+} pair [33].

Based on the above discussions, $0.675BiFeO_3$–$0.325PbTiO_3$ (BF–PT) is chosen as the starting component. Ceramics of B-site Cr-substituted BF–PT, $0.675BiFe_{1-x}Cr_xO_3$–$0.325PbTiO_3$ (BFC–PTx) ($x = 0.01$, 0.025, 0.05, 0.10), were prepared by solid state reaction method. The microstructures, dielectric, ferroelectric and magnetic properties were investigated systematically. It is shown that Cr-substitution can enhance room temperature ferroelectric and magnetic properties simultaneously. The underlying mechanism for enhanced multiferroic property was discussed.

2 Experimental procedure

Ceramics of pure BF–PT and BFC–PTx ($x = 0.01$, 0.025, 0.05, 0.10) were prepared by conventional solid-state reaction method. Metal oxides powders of Bi_2O_3 (99.0 %), Fe_2O_3 (99.0 %), PbO (99.0 %), TiO_2 (99.5 %), and Cr_2O_3 (99.0 %) were used as the staring reagents materials. The reagents in the stoichiometric ratio were mixed thoroughly in ethanol by ball milling for 24 h, dried and calcined at 800 °C for 2 h. Then the powder was ball milled for 24 h and dried again. The obtained powders were pressed into disks with diameter of 10.0 mm and thickness of about 1.0 mm and then sintered in covered alumina crucibles at 1000 °C for 2 h. To prevent the volatility of Bi and Pb, the disks were embedded in the powders during sintering. Thermal quenching experiments were performed by introducing a sintered disk into a furnace at 750 °C where it was held for 15 min, after which it was immediately immersed into water.

The phase of ceramics was characterized by powder X-ray diffraction (XRD, Rigaku Ultima, 40 kV, 40 mA) using crushed, unpoled ceramics. The microstructure morphology was observed by scanning electron microscopy (SEM, XL 30 FEG, Philips). Temperature dependent dielectric constant (ε_r) and dielectric loss (tanδ) were measured by using impedance analyzer (AgilentE4980AL). Before piezoelectric measurement, the ceramics were poled under 55–60 kV/cm in silicone oil for 20 min at room temperature and the piezoelectric coefficients d_{33} were measured using a Berlincourt d_{33} m (Institute of Acoustic, Chinese Academic Society, ZJ-6A, China). Ferroelectric polarization–electric field loops (P–E) were measured in a silicone oil bath at a frequency of 1 Hz by using a TF analyzer 1000 (aixACCT).Piezoelectric property (d_{33})were Magnetization-magnetic field (M–H) loops were measured by using a magnetic property measurement system (MPMS3, Quantum Design).

3 Results and discussion

The XRD patterns of all ceramics are shown in Fig. 1. As we can see, the MPB has been obtained in the pure BF–PT, with the coexistence of rhombohedral (R) phase and

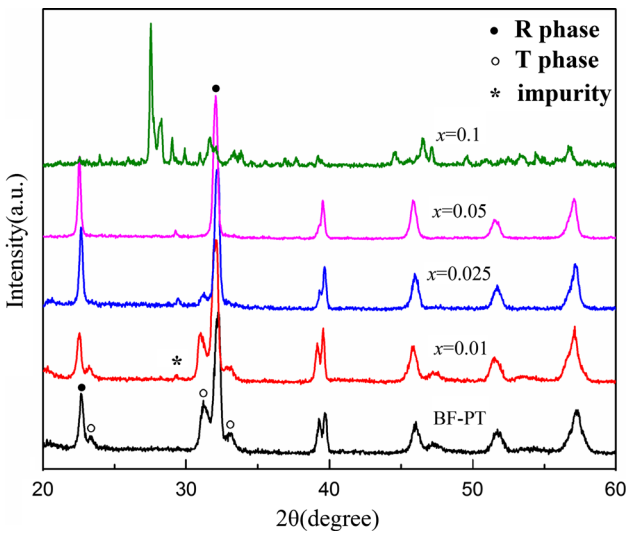

Fig. 1 X-ray diffraction patterns of the pure BF–PT and BFC–PTx ceramics ($x = 0.01$, 0.025, 0.05 and 0.1)

tetragonal (T) phase without any detectable impurities [26]. However, B-site Cr-substitution can induce a weak impurity diffraction peak locating around $2\theta \sim 29.4°$, this impurity peak becomes strong when the amount of Cr-substitution is increased. This impurity cannot be attributed to Cr_2O_3 or perovskite, thus may have very limited effect on multiferroic properties [34, 35]. It is interesting to note that the R phase becomes to be dominating gradually with the increase of Cr content. When x reaches 0.05, only diffraction peaks from R phase can be detected. This observation confirms that Cr has entered into the lattice and can change the structure form tetragonal phase to rhombohedral phase. Actually, it is reported that the tetragonality tends to decrease and the structure tends to change from tetragonal to rhombohedral when Cr^{3+} is diffused into $PbTiO_3$ lattice [36]. It should be noted that higher Cr content, for example, $x = 0.10$, will lead to considerable non-perovskite phases, as evidenced by the XRD patterns shown in Fig. 1. This observation indicates that the solution limit is close to $x = 0.05$. Accordingly, the following property measurements will focus on the compositions with $x \leq 0.05$.

Figure 2a–d shows the microstructure morphologies of the ceramics recorded by SEM. Clearly, all the ceramics are well sintered and have dense microstructures without cracks. The average grain size of BF–PT is $\sim$1.5 μm. However with the increase of Cr content, the grain size decreases monotonously with the average grain size of $\sim$1.0, $\sim$0.8 and $\sim$0.5 μm for $x = 0.01$, 0.025, 0.05, respectively.

The temperature dependent dielectric constant (ε_r) and dielectric loss (tanδ) of all samples measured at 1 MHz are shown in Fig. 3a–b. Two important features about Fig. 3a should be addressed. First, the ferroelectric T_c of pure BF–PT is 666 °C, and it slightly decreases to 656, 652, 642 °C for $x = 0.01$, 0.025, 0.05, respectively. The decreased ferroelectric T_c confirms the B-site substitution of Cr for Fe/Ti again [37], because if Cr cations have not entered into the BF–PT lattice but exist as isolated second particles in BF–PT matrix, the ferroelectric T_c should be composition-independent. The ferroelectric T_c has not decreased significantly because the Cr content is too low. Second, the peak ε_r value has changed obviously. The ε_r firstly increases from 7310 for BF–PT to 7450 for $x = 0.01$, then decreases to 5931 and 4645 for $x = 0.025$ and 0.05 respectively. Dielectric property is a very complex issue since many parameters like grain size, domain wall and domain switching, etc. have contributions to dielectric constant. To explain our observation, two main contributions from ferroelectric polarization effect and grain size effect should be considered [38, 39]. The slight increase of dielectric constant is attributed to Cr-substitution enhanced ferroelectric polarization, while the following decreased dielectric constant with further increasing Cr content is attributed the decreased grains size, in spite of the enhanced polarization. In general, BF–PT based ceramics show relatively large dielectric loss at high temperature [40]. However, as can be seen from Fig. 3b, on the one hand, all ceramics show low dielectric loss at room temperature, the dielectric loss increases with increasing

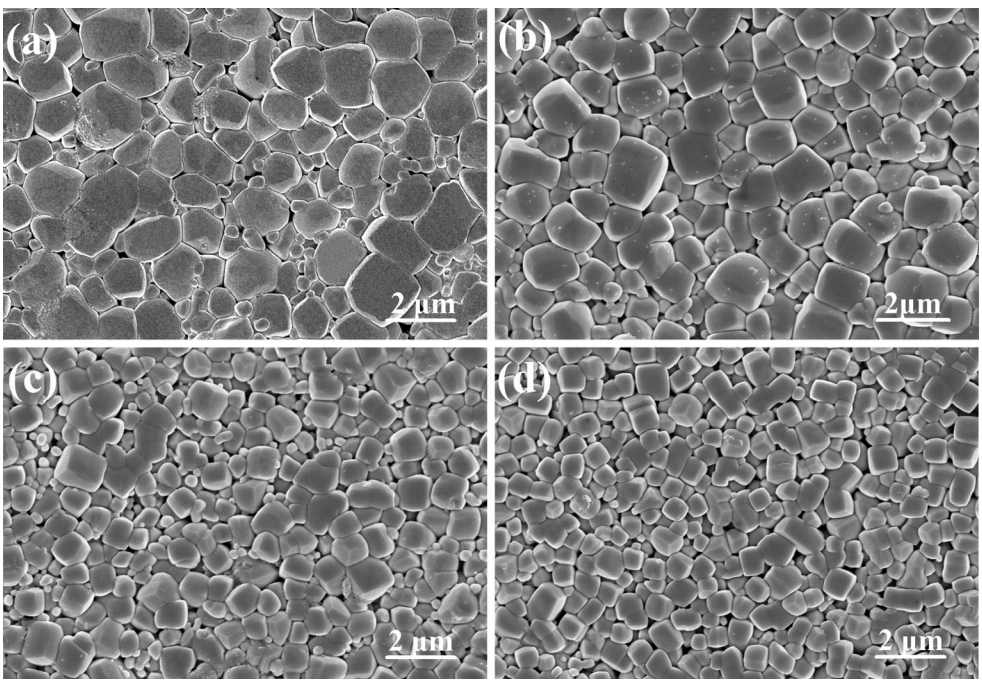

Fig. 2 SEM micrographs of the pure BF–PT and BFC–PTx ceramics **a** pure BF–PT, **b** $x = 0.01$, **c** $x = 0.025$, and **d** $x = 0.05$

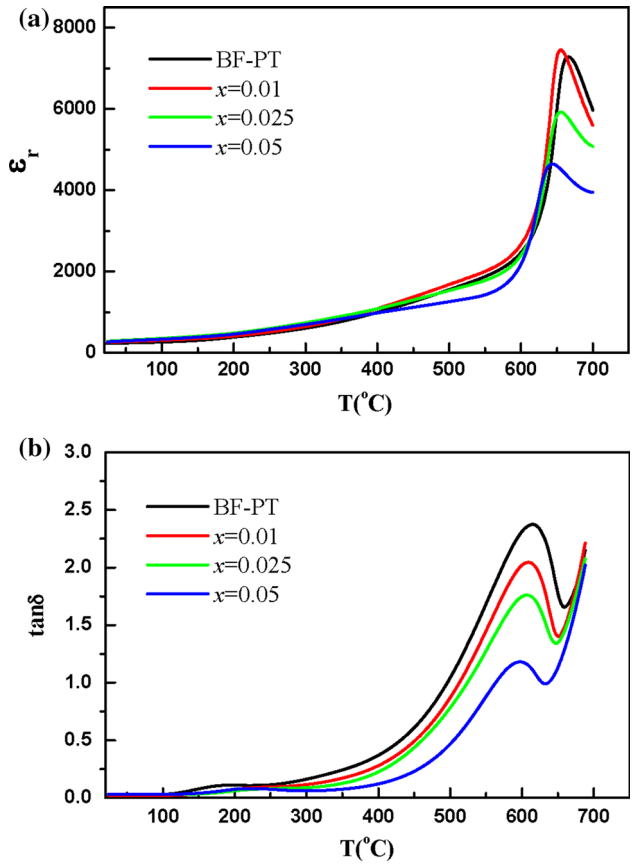

Fig. 3 Temperature dependent dielectric constant (ε_r) and dielectric loss (tanδ) of the pure BF–PT and BFC–PTx ceramics ($x = 0.01$, 0.025, 0.05)

temperature, reaching the maximum close to ferroelectric T_c. The observed further increasing dielectric loss should be attributed to thermal-activated defects. And on the other hand, Cr-substitution suppresses the dielectric loss significantly, which may be the result of Cr-substitution-reduced oxygen vacancy concentration. The suppressed dielectric loss indicates the increased resistivity, which is beneficial for investigating the intrinsic ferroelectric properties, as will be shown below. Further detailed investigations on dielectric properties are underway.

Figure 4 plots the piezoelectric coefficient d_{33} of the BF–PT and BFC–PTx ($x = 0.01$, 0.025, 0.05) ceramics, respectively. The d_{33} increases monotonously from 34 pC/N for BF–PT to 60 pC/N for $x = 0.05$ sample. We could explain the phenomenon as follows: The first one is the suppressed conductivity, which is caused by the reduction of oxygen vacancy concentration, and can be helpful to release ferro/piezoelectric property [41]. The second is the influence of grain size, small grains can be partially attributed to small domain size and piezoelectric-related constants increase with decreasing domain size, so it would have positive effect on d_{33} [42, 43].

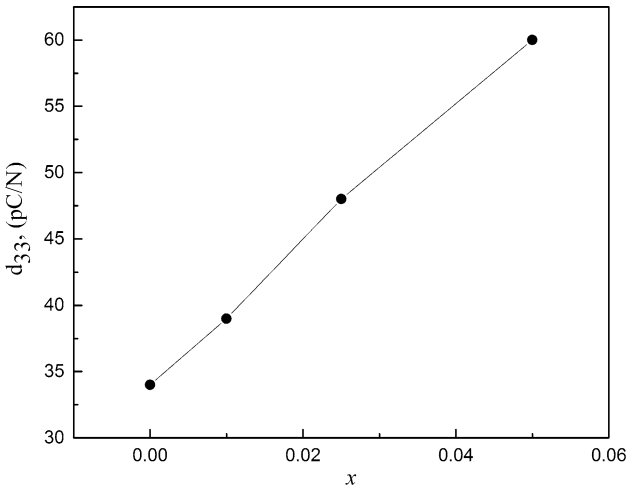

Fig. 4 Piezoelectric coefficient d_{33} of the pure BF–PT and BFC–PTx ceramics ($x = 0.01$, 0.025, 0.05)

The ferroelectric P–E loops obtained at 4.0 kV/mm of pure BF–PT and BFC–PTx ($x = 0.01$, 0.025, 0.05) ceramics are plotted in Fig. 5a. As can be seen, the pure BF–PT has a quite low remnant polarization and saturated polarization of 0.40 and 1.60 μC/cm^2, respectively, consistent with other reports on un-quenched BF–PT ceramics [7]. The suppressed ferroelectricity of un-quenched BF–PT is due to that the existing defect dipoles can pin the domain walls, thus prevents the switching of domains. However, by B-site Cr-substituting, both the remnant polarization and saturated polarization are increased obviously. The ceramic of $x = 0.05$ has the largest remnant polarization and saturated polarization value of 2.3 and 4.3 μC/cm^2, about 6 and 3 times larger than that of pure BF–PT. This observation is reasonable since the Fe^{2+} is unavoidable [44], which induces oxygen vacancy for charge balance, thus dipoles are formed to suppress ferroelectricity. However, Cr-substitution can suppress the Fe^{2+} content, and thus suppress the defect dipoles content, therefore improve the ferroelectric behavior. Both the ferroelectric hysteresis loops of as-prepared and quenched BF–PT samples are comparatively shown in Fig. 5b, the BF–PT sample show much improved ferroelectric loop. It suggests that quenching from temperature above the T_c is an effective way to release the domain walls that were clamped by defects. However, after many experiments, we found quenching process cannot improve the ferroelectric loops of BFC–PT ($x > 0$) samples. The reason might be due to that B-site Cr-substitution can also improve the ferroelectricity of samples, and such Cr-substitution effect is similar as or better than the effect of quenching, thus further quenching the BFC–PT ($x > 0$) samples cannot improve the ferroelectricity again.

Figure 6a–d illustrates the room temperature magnetic M–H curves of the BF–PT and BFC–PTx ($x = 0.01$, 0.025,

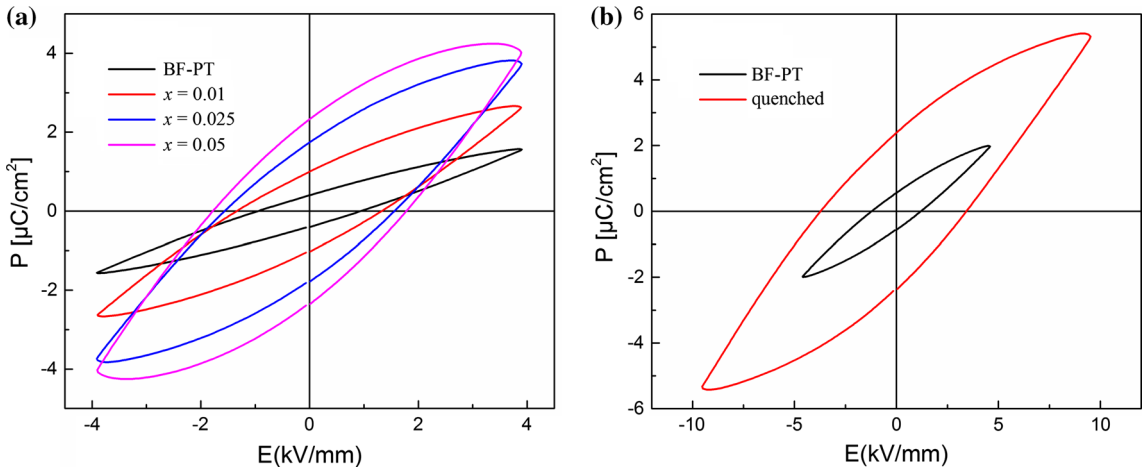

Fig. 5 **a** Ferroelectric hysteresis loops of the BFC–PTx ceramics ($x = 0$, 0.01, 0.025, 0.05), **b** ferroelectric hysteresis loops of BF–PT ceramic before and after quenching

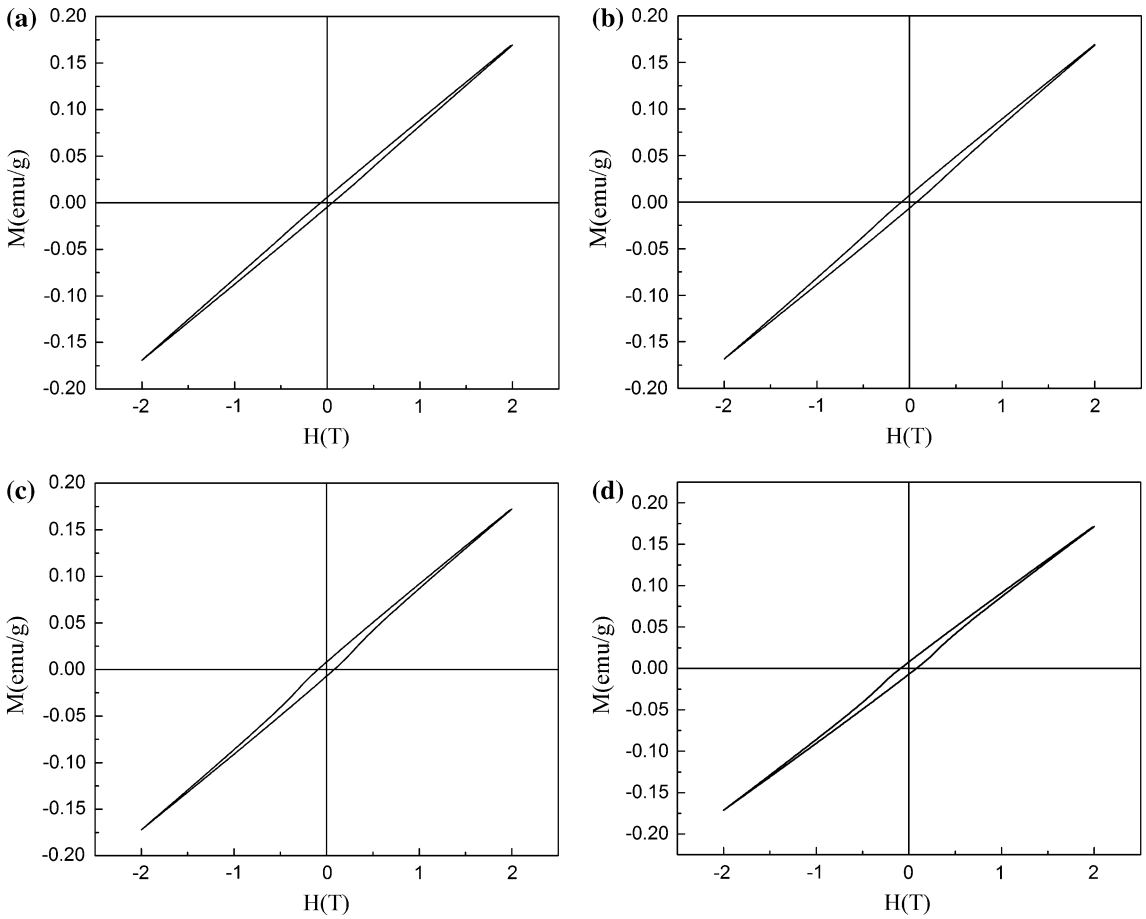

Fig. 6 Room temperature *M-H* curves of the pure BF–PT and BFC–PTx ceramics, **a** BF–PT, **b** $x = 0.01$, **c** $x = 0.025$, and **d** $x = 0.05$

0.05) ceramics, respectively. All ceramics exhibit slim nonlinear hysteresis loops with observable switchable magnetization, indicating the weak ferromagnetic behavior. It is noted that the maximum magnetization is almost composition-independent with the value of 0.17 emu/g. This is attributed to the fact that the macroscopic antiferromagnetic order is not changed since Cr content is still too low. However, the pure BF–PT ceramic exhibits the lowest remnant magnetization of 0.005 emu/g, with increasing Cr-content, the remnant magnetization tends to increase with

the value of 0.007, 0.009, 0.009 emu/g for $x = 0.01$, 0.025, and 0.05, respectively. In general, pure BF–PT has antiferromagnetic order and the remnant magnetization should be zero. However, our BF–PT has observable remnant magnetization, which is attributed to two factors. One is that the Fe^{2+} cannot be eliminated completely [40], which leads to oxygen vacancies appearance, such oxygen vacancies can induce weak room temperature ferromagnetic behavior [45, 46]. And the other factor is that the introduction of PT into BF can destruct the spin cycloid of BF to enhance ferromagnetic property [47]. The increased remnant magnetization with increasing Cr content is due to the formed local magnetic interaction between Fe^{3+} and Cr^{3+}. By noting that the spin configuration of Fe^{3+} and Cr^{3+} (Fe^{3+}: $3d^5$, $S = 5/2$, Cr^{3+}: $3d^3$, $S = 3/2$), they can form either ferromagnetic Fe(↑↑↑↑↑)–Cr(↑↑↑) or antiferromagnetic Fe(↓↓↓↓↓)–Cr(↑↑↑) configurations, leading to theoretical net magnetization of either 8.0 or 2.0 μ_B/f.u., respectively. In our cases, such ferro/ferrimagnetic Fe^{3+}–Cr^{3+} patches are embedded in the antiferromagnetic matrix, and higher Cr content, more ferro/ferrimagnetic Fe^{3+}–Cr^{3+} patches. Therefore, it is reasonable that the remnant magnetization increases with increasing Cr content.

4 Conclusion

In summary, single phase pure BF–PT and B-site Cr-substituted BFC–PTx ($x = 0.01$, 0.025, 0.05,) were prepared by solid-state reaction method and investigated. Both the room temperature ferroelectric and magnetic properties can be enhanced simultaneously by the Cr-substitution. The underlying mechanism is due to that Cr-substitution can suppress the defect dipoles, which releases ferroelectricity, and that the formed local Fe^{3+}–Cr^{3+} ferromagnetic/ferrimagnetic patches, which are embedded in the antiferromagnetic matrix to improve magnetization. We believe our results are helpful for developing room temperature multiferroic materials with improved switchable polarization and magnetization.

Acknowledgments This work was supported by the 973 Program (2013CB632900, 2015CB921203), the National Nature Science Foundation of China (U1432112), and "Dengfeng B" project of Nanjing University.

References

1. W. Eerenstein, N.D. Mathur, J.F. Scott, Nature **442**, 759 (2006)
2. H. Zheng, J. Wang, S.E. Lofland, Z. Ma, L. Mohaddes-Ardabili, T. Zhao, L. Salamanca-Riba, S.R. Shinde, S.B. Ogale, F. Bai, D. Viehland, Y. Jia, D.G. Schlom, M. Wuttig, A. Roytburd, R. Ramesh, Science **303**, 661 (2004)
3. C.W. Nan, I.M. Bichurin, S. Dong, D. Viehland, G. Srinivasan, J. Appl. Phys. **103**, 031101 (2008)
4. Y. Wang, Q. Hui, J. Hong, C. He, C.W. Nan, Appl. Phys. Lett. **88**, 142503 (2006)
5. S. Dong, J.F. Li, D. Viehland, J. Cheng, L.E. Cross, Appl. Phys. Lett. **85**, 3534 (2004)
6. V. Kothai, A. Senyshyn, R. Ranjan, J. Appl. Phys. **113**, 084102 (2013)
7. M.W. Zhu, Z.G. Ye, Appl. Phys. Lett. **89**, 232904 (2006)
8. E. VenkataRamana, S.V. Suryanarayana, T. BhimaSankaram, Solid State Sci. **12**, 956 (2010)
9. R.R. Raut, P.H. Salame, J.T. Kolte, C.S. Ulhe, P. Gopalan, J. Mater. Sci. Mater. Electron. **27**, 730 (2016)
10. G.L. Yuan, K.Z. Baba-Kishi, J.-M. Liu, S.W. Or, Y.P. Wang, Z.G. Liu, J. Am. Ceram. Soc. **89**, 3136 (2006)
11. C. Lan, Y. Jiang, S. Yang, J. Mater. Sci. **46**, 734 (2011)
12. G.L. Yuan, D.S.W. Or, J.M. Liu, Z.G. Liu, Appl. Phys. Lett. **89**, 1 (2006)
13. R.K. Mishra, D.K. Pradhan, R.N.P. Choudhary, A. Banerjee, J. Magn. Magn. Mater. **320**, 2602 (2008)
14. A. Agarwal, S. Sanghi, J. Appl. Phys. **110**, 073909 (2011)
15. Q. Zheng, Y. Guo, F. Lei, X. Wu, D. Lin, J. Mater. Sci. Mater. Electron. **25**, 2638 (2014)
16. Y.F. Cui, Y.G. Zhao, L.B. Luo, J.J. Yang, H. Chang, M.H. Zhu, D. Xie, T.L. Ren, Appl. Phys. Lett. **97**, 222904 (2010)
17. C. Zhou, H. Yang, Q. Zhou, G. Chen, W. Li, H. Wang, J. Mater. Sci. Mater. Electron. **24**, 1685 (2013)
18. Q. Fan, C. Zhou, Q. Li, J. Xu, C. Yuan, G. Chen, J. Mater. Sci. Mater. Electron. **26**, 9336 (2015)
19. V.A. Khomchenko, D.A. Kiselev, J.M. Vieira, L. Jian, A.L. Kholkin, A.M.L. Lopes, Y.G. Pogorelov, J.P. Araujo, M. Maglione, J. Appl. Phys. **103**, 24105 (2008)
20. X.D. Qi, J. Dho, R. Tomov, M.G. Blamire, J.L. MacManus-Driscoll, Appl. Phys. Lett. **86**, 062903 (2005)
21. J.Y. Zhang, J. Luo, J.B. Li, J.K. Liang, Y.C. Wang, L.N. Ji, Y.H. Liu, G.H. Rao, J. Alloys Compd. **469**, 15 (2009)
22. Y.H. Gu, Y. Wang, F. Chen, H.L. Chan, W. Chen, J. Appl. Phys. **108**, 1 (2010)
23. N. Wang, J. Cheng, A. Pyatakov, A.K. Zvezdin, J.F. Li, L.E. Cross, D. Viehland, Phys. Rev. B **72**, 104434 (2005)
24. P. Hu, J. Chen, J. Deng, X. Xing, J. Am. Chem. Soc. **132**, 1925 (2010)
25. L. Fan, J. Chen, S. Li, H. Kang, L. Liu, L. Fang, X. Xing, Appl. Phys. Lett. **102**, 022905 (2013)
26. H. Amorín, C. Correas, P. Ramos, T. Hungría, A. Castro, M. Algueró, Appl. Phys. Lett. **101**, 172908 (2012)
27. C. Correas, T. Hungría, A. Castro, J. Mater. Chem. **21**, 3125 (2011)
28. J. Zhuang, H. Wu, W. Ren, Z.G. Ye, J. Appl. Phys. **116**, 066809 (2014)
29. J. Zhuang, L.W. Su, H. Wu, A.A. Bokov, M. Liu, W. Ren, Z.G. Ye, Appl. Phys. Lett. **107**, 182906 (2015)
30. V. Reddy, K.C. Sekhar, N. Dabra, A. Nautiyal, J.S. Hundal, N.P. Pathak, R. Nath, ISRN Mater. Sci. **2011**, 142968 (2011)
31. K. Udea, H. Tobata, T. Kawai, Science **280**, 1064 (1998)
32. J. Hong, A. Stroppa, J. Íñiguez, S. Picozzi, D. Vanderbilt, Appl. Phys. Lett. **85**, 054417 (2012)
33. P. Baettig, C. Ederer, N.A. Spaldin, Phys. Rev. B **72**, 214105 (2005)
34. X.H. Liu, Z. Xu, X.Y. Wei, X. Yao, J. Am. Chem. Soc. **91**, 3731 (2008)
35. M. Sahni, S. Singh, R. Bhargava, A.K. Chawla, R. Chandra, A. Dalvi, N. Gupta, S. Kumar, N. Kumar, J. Supercond. Nov. Magn. **26**, 397 (2013)
36. C.I. Cheon, J.S. Park, J. Mater. Sci. Lett. **16**, 2043 (1997)

37. L. Wu, Y.Y. Lee, C.K. Liang, T.S. Wu, Jpn. J. App. Phys. **31**, 3913 (1992)
38. J.G. Chen, Y.F. Qi, G.Y. Shi, X.L. Yan, S.W. Yu, J.R. Cheng, J. Appl. Phys. **104**, 4124 (2008)
39. Y. Sudo, M. Hagiwara, S. Fujihara, Ceram. Int. **42**, 8206 (2016)
40. Y.Q. Guo, P. Xiao, R. Wen, Y. Wan, Q.J. Zheng, D.L. Shi, K.H. Lam, M.L. Liu, D.M. Lin, J. Mater. Chem. C **3**, 5811 (2015)
41. J.R. Cheng, Z.Y. Meng, L. Eric Cross, J. Appl. Phys. **96**, 6611 (2004)
42. H. Takahashi, Y. Numamoto, J. Tani, K. Matsuta, J. Qiu, S. Tsurekawa, Jpn. J. App. Phys. **45**, 30 (2005)
43. T. Karaki, K. Yan, M. Adachi, Jpn. J. App. Phys. **46**, 7035 (2007)
44. T.J. Park, G.C. Papaefthymiou, A.J. Viescas, A.R. Moodenbaugh, S.S. Wong, Nano Lett. **7**, 766 (2007)
45. G. Bouzerar, T. Ziman, Phys. Rev. Lett. **96**, 207602 (2006)
46. M. Venkatesan, C.B. Fitzgerald, J.M.D. Coey, Nature **430**, 630 (2004)
47. J.R. Cheng, S.W. Yu, J.G. Chen, Z.Y. Meng, L.E. Cross, Appl. Phys. Lett. **89**, 2911 (2006)